Published in final edited form as:
J Phys Chem B. 2007 February 1; 111(4): 800–810. doi:10.1021/jp0659608.

Structure of Radicals from X-irradiated Guanine Derivatives: An Experimental and Computational Study of Sodium Guanosine Dihydrate Single Crystals

Nayana Jayatilaka and **William H. Nelson**
Department of Physics and Astronomy Georgia State University P.O. Box 4106 Atlanta, GA 30302-4106 USA

Abstract

In sodium guanosine dihydrate single crystals, the guanine moiety is deprotonated at N1 due to growth from high-pH (>12) solutions. EPR and ENDOR study of crystals x-irradiated at 10 K detected evidence for three radical forms. Radical R1,characterized by two proton and two nitrogen hyperfine interactions, was identified as the product of net hydrogenation at N7 of the N1-deprotonated guanine unit. R1 exhibited an unusually distorted structure leading to net positive isotropic components of the hydrogen couplings. Radical R2, characterized by one proton and one nitrogen hyperfine coupling was identified as the primary electron loss product. This product is equivalent to that of deprotonation at N1 by the guanine cation and represents the first ENDOR characterization of that product. Radical R3, characterized by a single hydrogen hyperfine coupling, was identified as the product of net dehydrogenation at C1 of the ribose moiety. The identification of radicals R1-R3 was supported by DFT calculations on several possible structures using the B3LYP/6-311G(2df,p)//6-31G(d,p) approach. Radical R4, detected after warming the crystals to room temperature, was identified as the well-known product of net hydrogenation of C8 of the (N1-deprotonated) guanine component. Radical R1, evidently formed by protonation of the primary electron addition product, was present as roughly 60% of the total radicals detected at 10 K. Radical R2 was present as roughly 27% of the total yield, and the concentration of R3 contributed the remaining 13%. R3 is evidently the product of oneelectron oxidation followed by deprotonation; thus, the balance of oxidation and reduction products is approximately equal within experimental uncertainty.

1. Introduction

Of all the components of DNA, guanine is perhaps the most highly studied. A major reason is its well-documented status as the component with the lowest ionization potential, and therefore as the most easily oxidizable of the DNA bases. Nearly fifty years ago, using quantum biochemistry methods available at the time, Pullman and Pullman noted about a group of purines and pyrimidines including the DNA bases that “The best electron donor among these bases should be guanine”. [1] In their analysis of radicals formed in oriented strands of DNA, Gräslund, *et al*., used this computation-based idea in concluding that the primary guanine electron-loss product was most probably a major contributor to the EPR spectra.[2]

Corresponding author: William H. Nelson Department of Physics and Astronomy P.O. Box 4106 Georgia State University Atlanta, GA 30302-4106 US Ph: 404-651-1970 FAX: 404-651-1427 e-mail: E-mail: wnelson@gsu.edu.

Supporting Information Available
Supporting information is available and includes figures showing the WINSIM fits to experimental spectra from six different crystal orientations (Figure S1), the angular dependence of the data and fit for coupling tensors R1 (Figure S2), R2 (Figure S3), R3 (Figure S4), and R4 at room temperature (Figure S5). This material is available free of charge via the Internet at http://pubs.acs.org.

With this evidence that electron loss in DNA occurs mainly at guanine residues, the initial chemical properties of the guanine cation became a topic of significant interest. Because loss of an electron reduces the amount of negative charge in a molecule, it is inevitable that it will reduce the strength of bonds in guanine with the greatest degree of ionic character. Since these involve the N-H hydrogens, it seemed reasonable to expect the guanine cation to easily deprotonate, if it did not spontaneously do so. Therefore, one question which arose was whether or not the guanine product detected in DNA was the formal cation or its deprotonated product.

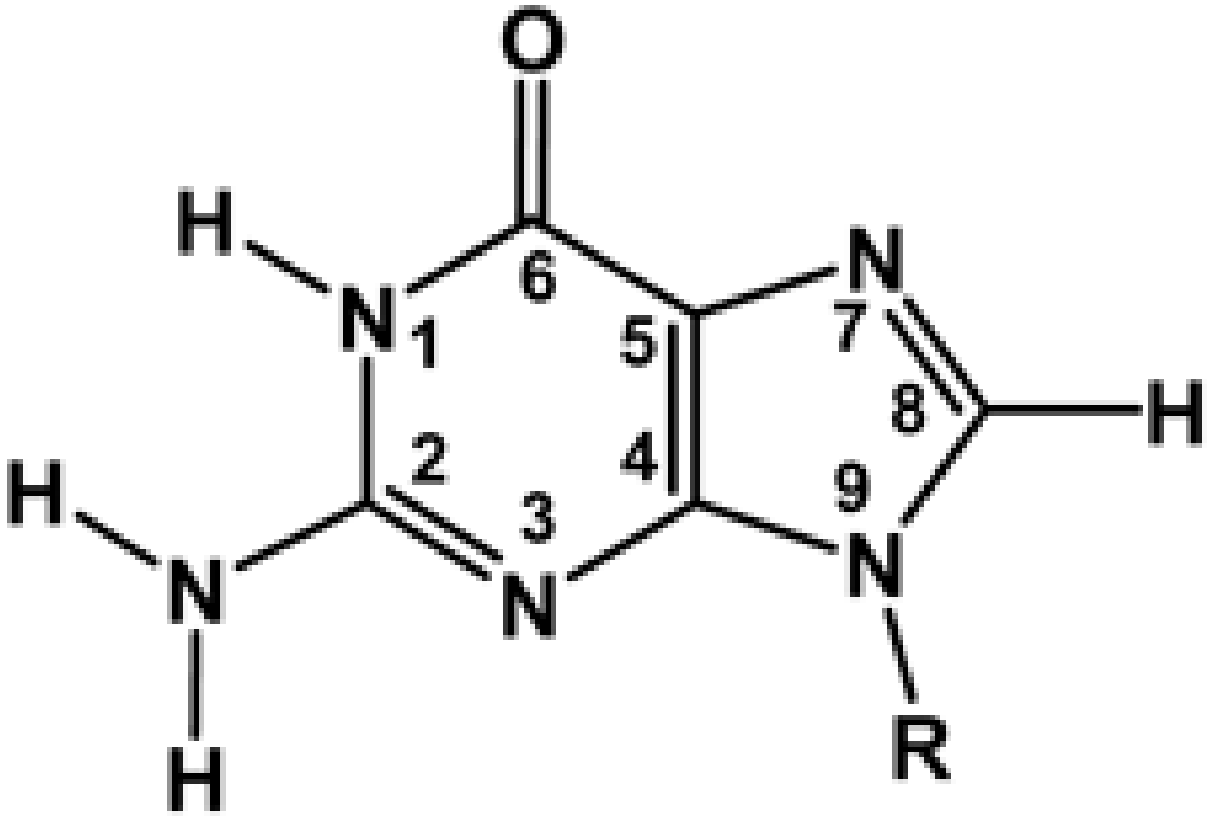

Guanine

A study employing single crystals of guanine grown from acidic solution, causing protonation at N7, reported the magnetic parameters of the formal guanine cation.[3] In this system, electron loss led directly to deprotonation of the acidic N7 proton. The deprotonation occurred at 10K, a behavior indicating little or no barrier to this process. As well, this generally reinforced the idea that the primary electron loss products readily deprotonated. Shortly thereafter, a pair of studies employing deoxyguanosine monophosphate (dGMP) single crystals reported spectra and magnetic parameters from deprotonated guanine oxidation products. However, the two groups arrived at different conclusions for the identity of the product: on the basis of EPR spectra, one concluded that guanine deprotonated at N1;[4] on the basis of detailed EPR/ENDOR data, the other concluded that deprotonation occurred at the exocyclic amino.[5] A study of

guanine derivatives in aqueous solution using pulse radiolytic techniques concluded that one-electron oxidized guanine deprotonated at N1 under those conditions.[6] As well, an early HF / *ab initio* set of calculations concluded that the N1-deprotonated structure is more stable than the amino-deprotonated version,[7] while more recent DFT and molecular dynamics calculations led to the opposite conclusion.[8] For the case of one-electron-oxidized guanine within DNA, where it is paired with cytosine, computational results are similarly ambivalent regarding whether or not deprotonation occurs at all: Hutter and Clark concluded that transfer of a proton from N1 of guanine to N3 of cytosine is unfavorable by *ca*. 1.6 kcal/mol,[9] and more recent calculations by Li, *et al.*, found the lower value of 1.25 kcal/mole leading them to suggest that an equilibrium exists between initial and transferred states with little difference in populations of the two.[10] Therefore, despite these reports, the question remains as to the position at which one-electron oxidized guanine is likely to deprotonate in DNA, and if it will do so at all.

EPR methods provide the most direct approach to identifying the protonation state of the guanine radical in DNA. The detailed EPR/ENDOR study of dGMP, and subsequent study of 3′,5′ cyclic guanosine monophosphate (cGMP),[11] provided a good set of magnetic parameters for the amino-deprotonated product. However, no such set of magnetic parameters is available for the N1-deprotonated product. The “guanine signal” in the EPR spectrum from irradiated DNA has only the suggestion of hyperfine structure. In addition, the EPR parameters of the N1-deprotonated product are very similar to those of the formal cation. Thus, it is virtually impossible to distinguish spectra from the two structures directly from irradiated DNA without prior information of the magnetic parameters. Therefore, since no such experiment-derived parameters exist for the N1-deprotonated product of the guanine cation, we undertook a study of sodium guanosine dihydrate (NaGR) single crystals with the goal of providing these.

In the NaGR system, created by crystallizing guanosine from high-pH NaOH solution, the guanine base exists as a formal anion due to deprotonation at N1 (Structure 1). The rationale for this study was that the N1-deprotonated radical in this system is the primary electron-loss product of the parent guanine base. Previous study of sodium inosine crystals, prepared in a similar fashion from high-pH solutions, found that the primary electron-loss product was stabilized in the crystal and thereby suggested that the corresponding product would be stabilized in the NaGR system.[12] As will be described below, the experimental results in fact provided the sought-after magnetic hyperfine parameters for the N1-deprotonated guanine radical along with evidence for an additional product of electron loss. As well, the results also showed that the primary electron-gain product protonated at N7, with little or no activation barrier, leading to a radical with a very unusual geometry in comparison to those usually found in irradiated purines.

2. Experimental

Guanosine (GR) powder was obtained commercially (Sigma G6752) and used with no further purification. Single crystals of Na^+. guanosine$^-2H_2O$ (NaGR) were grown from a solution of guanosine in NaOH (*ca*. 0.6 M GR in *ca*. 0.75 N NaOH; pH >12). The mixture was first heated in an open beaker on a hotplate set to 130°C surface temperature (making the solution temperature about 85°C) for complete dissolution. The solution was then filtered and returned to the hotplate until the liquid was reduced to the point of saturation (indicated by the appearance of small crystals on the surface). Finally, the solution was transferred to a hotplate set to 65°C surface temperature (making the solution temperature about 40°C). Good crystals formed within approximately an hour.[13] Despite this extremely rapid growth rate, x-ray diffraction results and ENDOR spectra indicated insignificant disorder in the crystals.

Nagashima, *et al*.,[14] reported a full x-ray diffraction analysis of Na^+·guanosine$^-$·$2H_2O$ crystals and found them to be orthorhombic, belonging to space group $P2_12_12_1$, with unit cell

dimensions *a=10.433(5)* Å, *b=21.430(11)* Å and *c=6.355(3)* Å. The $P2_12_12_1$ cell contains four symmetry-related molecules. In the crystals, the guanine base exists as a formal anion from deprotonation at N1 as a result of growth from the highly basic solution, and the ribose is in the *syn* conformation with an intramolecular hydrogen bond between HO5′ and N3. Structure 1 shows these features and indicates the standard atomic numbering system. The diagram also indicates the system of hydrogen bonds and close contacts to neighboring units. Unit cell dimensions of the crystals used in these experiments measured by x-ray diffraction confirmed their identity. The experimental results are reported in an orthogonal *xyz* coordinate system based on the crystallographic *abc* axes.

Crystals selected for experiments were oriented by x-ray diffraction (Buerger precession) methods and transferred without loss of orientation to the spectrometer's crystal mount. After cooling to *ca*. 10K, the crystals were irradiated to a total dose of *ca*. 50kGy with 55 kVp x-rays from a W-target tube filtered by a 0.05mm Al-filter. Following irradiation and without warming, the crystals were inserted into the EPR resonator. EPR, ENDOR and ENDOR-Induced EPR (EIE) spectra were recorded at K-band (~23.7 GHz) for three independent rotations about <a>, <b> and <c>. Data were analyzed using the MAGRES program which incorporates a linear regression fitting technique[15] supplemented with non-linear methods for obtaining the final results and estimates of statistical uncertainties. Since the crystal system is orthogonal, data were also collected for rotation about <101*> to resolve the Schonland ambiguity.[16] The specific undamaged molecular directions were calculated using a modified version of the X-ray crystallographic program ORFEE.[17] EIE patterns from the ENDOR lines were used to assign sets of hyperfine couplings to individual radicals indicated by the spectra.

Radical structures and their geometries were tested with calculations using DFT methods included in Gaussian 03 for Windows (G03W).[18] All initial radical geometries were derived directly from the crystallographic coordinates and the NOSYMM keyword was used in the route section of each step to prevent shifting or rotating the Cartesian coordinates of the radical model with respect to the reference frame. In doing so, a direct link to the original crystal axes was preserved.[19] The structures were optimized as isolated molecules (gas-phase) and hyperfine coupling values were subsequently calculated using a higher basis set. Frequency calculations for the optimized structures were performed at the same level of theory as the optimizations to ensure that the molecular geometries represented true minima on the potential energy surfaces.

The choice of basis sets for guanine calculations was problematic in some cases since the parent structure is anionic. For gas-phase calculations, the common approach is to use basis sets including diffuse functions to properly describe the HOMO.[20] This is necessary because the HOMO of a molecular anion is less tightly bound and may extend much farther from the molecular framework than that of a neutral or cationic structure. Anionic structures based on guanine reflect this property and it is well known that the HOMO of these exhibits severe diffuse character when the computations include diffuse functions.[21] In fact, computational evidence at the present indicates that guanine anions may be stable in the gas phase only as dipole-bound structures.[22]

Experimental evidence also indicates that the situation is different in condensed media and that dipole-bound or extremely diffuse states are unrealistic for the condensed state. For example, Hendricks, *et al*., demonstrated experimentally that the dipole-bound state of uracil anions is suppressed by association with only a single water molecule.[23] Molecules trapped in crystals, such as those under study here, experience an electrostatic environment similar to that of solvation. Thus, in both cases, the electronic system is affected in such a way that the anions may exhibit a normal valence-bound character in condensed media—solvated or crystalline–thereby rendering the more realistic computational description that without diffuse functions.

The standard computational approach in this study was to optimize the geometries using the B3LYP functional and the 6-31G(d,p) basis set. Hyperfine coupling values were calculated subsequently using the 6-311G(2df,p) basis. Calculations using these sets including diffuse functions (the + and ++ variations) with some of the structures listed below in Table 2 led to results in which the HOMO exhibited severe diffuse character. As well, these results exhibited nonsense EPR characteristics. Repeating these computations using the PCM solvation method led to geometries and hyperfine parameters generally consistent with those from basis sets without diffuse functions. Therefore, our conclusion was that these computational observations, in combination with the previous experimental and computational work on molecules in condensed media, justifies the use of basis sets without diffuse functions for all structures tested in this study.

A caveat is that basis sets including diffuse functions may be necessary in some cases for properly describing molecular EPR properties in condensed media. This was demonstrated by previous work with sodium inosine in which the HOMO of the putative doubly-negative electron adduct of N1-deprotonated hypoxanthine apparently interacted with the electrostatic environment to a sufficient degree that the hyperfine couplings were significantly altered.[12] In this case, the electrostatic environment affected, but apparently did not completely suppress, the diffuse character of the HOMO. The experimental results were best modeled with diffuse functions using a structure placed into a continuous dielectric medium by means of the PCM solvation method. Thus, the computational method of accounting for effects of the electrostatic environment on the properties of molecules trapped in condensed media needs to be chosen carefully in each case.

For radical R2, g tensors were calculated using the NMR keyword of G03W. G03W reports the tensors as an asymmetric matrix trix g_{G03} which can be converted to the standard symmetrical form by constructing the product $g^2_{symm}=g_{G03}g^T_{G03}$.[24] The eigenvectors of g^2_{symm} are the same as those of g_{symm} and the eigenvalues of g_{symm} are the square roots of those from g^2_{symm}.

A series of EPR spectrum simulations was carried out to test the validity of the radical structures. Since the ENDOR provided only proton coupling values, it was necessary to estimate the nitrogen hyperfine contributions using values initially indicated by computation or the experimental spectra. For this purpose, the *WINSIM* program[25] was particularly useful since it includes an “optimize” feature that automatically adjusts the selected couplings, the g-shifts of selected radicals, and the relative concentrations of the radicals to obtain the best simulation of a specific experimental spectrum. The result of applying this procedure to a composite spectrum is a refined set of estimated nitrogen couplings and g-shifts. With these results from a set of EPR spectra, it is possible to test the self-consistency of the estimated couplings by calculating the indicated nitrogen hyperfine tensors. For the experiments reported here, the simulations were carried out for crystal orientations with the magnetic field along each crystallographic axis and at one known off-axis position in each crystallographic plane. (See Supplementary Figure S1.) The estimated radical concentrations were obtained from these nine data sets,[26] and the nitrogen couplings reported in the following tables were obtained from the data sets using procedures described previously.[27]

3. Results and Discussion

Fig. 1 shows EPR obtained from NaGR crystals immediately after irradiation at 10K. Also, ENDOR, EPR, and EIE patterns obtained with the magnetic field along the <b> crystallographic axis are shown in Fig. 2. The EIE patterns can be grouped into three distinct sets: lines 1a and 1b, line 2, and line 3. (The feature near 55 MHz in the ENDOR spectrum is

a spectrometer artifact.) These groupings indicate at least three radicals present at this temperature as will be discussed in detail below.

3.1 Radical R1: N7-protonated anion (N7-hydrogenation)

The two ENDOR lines labeled 1a and 1b in Fig. 2 yielded EIE patterns (Fig. 2) similar enough to conclude that they belong to the same radical species. Thus, they were associated with **R1** and were easily followed in the three planes. The overall width and substructure of these EIE patterns indicated that the ENDOR lines are associated with the prominent 12-line EPR pattern. Annealing experiments showed that these ENDOR lines gradually decayed upon warming the crystals and became undetectable around 100K with no detectable successors. Table 1 lists the hyperfine couplings extracted from analysis of these lines' angular dependence. (Complete angular dependence plots are shown in figure S2 of the supplementary materials.)

Although both $R1_a$ and $R1_b$ appear to have α-like properties, close inspection reveals a more unusual character for $R1_a$. Specifically, the magnitude of its isotropic component is 62.2 MHz and the magnitude of its dipolar component is 22.0 MHz. [28] Their ratio $\left|a_{iso}\right| \Big/ \left|a_{dip}\right| = 2.8$ is significantly larger than is typical for α-couplings, *ca*. 2.0.[29] Also, none of the experimental eigenvectors associated with $R1_a$ correlated well with X-H bond (X = C or N) directions in the undamaged molecule. Possibilities for a radical structure exhibiting two α-couplings and capable of producing a twelve-line EPR pattern are limited. For example, ribose-centered products of OH elimination from C2′, C3′, or C5′ will lead to eight lines at most.

Because guanine-centered radicals may include interactions with one or more of the nitrogens, it is more likely that such radicals will yield the observed EPR pattern. As well, hydrogen loss or gain by the guanine moiety can lead to radicals exhibiting two different α-couplings as observed. It is now well known that bending at the center of spin can lead the normally-negative a_{iso} of an α-coupling to become more positive and possibly reach a magnitude greater than that of the more common planar geometry.[30] Pyramidal character of X-H bonds in the radical can explain the lack of correlation between the experimental eigenvectors and X-H directions of the undamaged molecule. It is common that normally-planar structures become pyramidal upon addition of an electron or a hydrogen atom. For these reasons, we undertook a systematic computational survey of structures based on N1-deprotonated guanine following electron or hydrogen addition.

Table 2 shows results from the computational survey. (For these computations, the ribose at N9 was replaced with a hydrogen.) Of the results listed, only that from net H addition to N7 has two hydrogen α-couplings similar to the experimental results. As well, the computational results for the HN7-addition structure indicate two nitrogen couplings similar in magnitude to those found experimentally. The prediction of two resolvable nitrogen couplings is consistent with the EPR since the twelve-line character of the EPR indicates coupling to at least one nitrogen along with hydrogen couplings $R1_a$ and $R1_b$.[31]

For HN7 addition, the computational results in table 2 indicate positive isotropic values for HN7 and HC8. The possibility of positive isotropic values complicates the process of identifying the radical. For X-H α-couplings (with X = C or N), the observed value consists of isotropic and dipolar components.[29,32] The dipolar component has three principal values, b_+, b_0, and b_-. Of these, b_+ and b_- have roughly the same magnitudes, while that of b_0 is near zero. Important about these for radical identification purposes is that the eigenvector associated with $\widehat{V}_+$ closely parallels the X-H bond.[29,30] Normally, a_{iso} is negative[32] so that $\widehat{V}_+$ corresponds to the coupling eigenvalue with minimum magnitude. However, in the case that a_{iso} is positive, $\widehat{V}_+$ corresponds to the coupling eigenvalue with maximum magnitude. Thus, in this case, it is

necessary to establish the sign of the isotropic coupling in order to associate the correct coupling component with the X-H bond.[33]

For HC8 in this structure, in addition to the predicted positive isotropic coupling, the computations also predict the ratio $\frac{|a_{iso}|}{|a_{dip}|} \simeq 4$. Together, these features indicate significant pyrimidal character in the bonds to C8 in the (gas phase) optimized structure. In fact, the C8-HC8 bond is 44.95° from the normal to the N7-C8-N9 plane in the optimized structure; thus, C8-HC8 is out of this plane by 45.05°. Although the computed a_{iso} for HC8 is significantly larger in magnitude than that of $R1_a$, the computed dipolar values are comparable. Also, the eigenvectors associated with the maximum, mid, and minimum principal values of $R1_a$ ($\widehat{V}_{max}$, $\widehat{V}_{mid}$, and $\widehat{V}_{min}$) correspond well to the computed $\widehat{V}_+$, $\widehat{V}_0$, and $\widehat{V}_-$ vectors: the respective angular differences are 7°, 8°, and 9°. Thus, on a qualitative basis, the computed HC8 coupling appears a reasonable match to R_{1a} and is consistent with a_{iso} being positive.

As for HC8, the computed a_{iso} for HN7 is also positive and reflects that the N7-HN7 bond is 31.5° out of the C5-N7-C8 plane in the optimized structure. In this case, the ratio $\frac{|a_{iso}|}{|a_{dip}|} \simeq 1$, a value reasonably consistent with typical N-H α-couplings. The computed a_{iso} is comparable in magnitude with $R1_b$ while the dipolar values of $R1_b$ are approximately 0.75 those from computation. The computed eigenvectors for HN7 and those for $R1_b$ (when treating the experimental a_{iso} as positive) compare reasonably well: the respective angular differences between $\widehat{V}_{max}$ and $\widehat{V}_+$, $\widehat{V}_{mid}$ and $\widehat{V}_0$, and $\widehat{V}_{min}$ and $\widehat{V}_-$ are 10°, 18°, and 19°. We note that the computed and experimental eigenvectors compare better when the experimental a_{iso} is taken to be negative: the respective angular differences are 10°, 9°, and 2°.[34] (We note also that taking a_{iso} as negative makes the two smaller dipolar components also negative and leads to better correspondence with the computational results.) However, a negative a_{iso} indicates a nearly planar arrangement of C5, N7, C8, and HN7. Manual adjustment of the N7-HN7 bond to bring it near enough to the C5-N7-C8 plane that the computed a_{iso} is negative and approximate in magnitude to the experimental value also leads to computed eigenvectors in much poorer agreement with experiment. Nevertheless, on the basis of the better eigenvector agreement, we conclude that the computed HN7 coupling best matches the experimental results for the case that a_{iso} is positive and the N7-HN7 bond is bent out of the plane.

We attribute the poorer agreement (magnitude and direction) between $R1_b$ and the HN7 coupling to the effects of interactions between the HN7 proton and neighboring molecules. Since the proton must have been transferred from a neighboring molecule following electron addition, a residual interaction with the original site is to be expected. For that reason, it also cannot be ruled out that a_{iso} for $R1_b$ is actually negative and that the residual intermolecular interaction in the crystal might counteract the intramolecular influences causing to pyramidal character of the N7 bonding system in the vacuum-state.

In the optimized structure, a_{iso} values for both HC8 and HN7 are strongly dependent on the out-of-plane character of their bonds. With the degree of non-planarity present in R1, the computed isotropic couplings are highly sensitive to the out-of-plane angle. Consequently, the geometry requires only a slight manual adjustment for the computed values to more closely match experiment. For example, adjusting the out-of-plane angle for HC8 to 40° (from 45°), without changing that of HN7, reduces the computed HC8 isotropic value from +83.5 to +64.3 MHz, a value more consistent with the experimental results. Figure 3 shows the as-optimized structure in several views while Table 3 shows a comparison between the experimental results, the computed results for the as-optimized structure, and those for the adjusted structure.

Besides these two proton couplings, the twelve-line character of the EPR and EIE patterns found with the magnetic field along the crystallographic <b> axis indicates at least one nitrogen coupling. Using the spectrum-fitting procedure described above, it was possible to estimate coupling tensors of the two nitrogen interactions listed in Table 2. These are consistent with the computed nitrogen couplings within the fairly large uncertainty associated with the experimental method.

In summary, therefore, the radical structure resulting from protonation at N7 of the primary electron gain product best fits the experimental and computational results. This is shown as Structure 2. This is an unusual structure exhibiting α-couplings from extremely non-planar X-H fragments. Although it was proposed many years ago [35] that such non-planarity could lead to the isotropic component of α-couplings becoming more positive and possibly changing sign, R1 is the most extreme and clear-cut example demonstrating this behavior of which we are aware.

3.2 Radical R2: Electron-loss product

ENDOR line 2 in Fig. 2 was assigned to radical **R2**. Line 2 was observed immediately after irradiation at 10 K; upon warming, the line began to decay at 40K but was detectable up to 200K. No successor radicals were detected during or following the warming process. (A complete angular dependence plot is shown in Figure S3 of the supplementary materials.) The hyperfine coupling extracted from analysis of the angular dependence is presented in Table 4. (The nitrogen coupling shown was obtained by the EPR spectrum simulation method.) Figure 4 shows the EIE from R2 compared to the simulated EPR for the magnetic field along <b> with the ENDOR coupling for line 2 and the nitrogen coupling listed in Table 4.

Coupling R2 is typical of that from a π-type α-proton. Eigenvector $\widehat{V}_{min}$ of the minimum principal value is 8.9° from the crystallographic C8-H bond direction and that of $\widehat{V}_{mid}$ is 8.1° from the ring perpendicular. On the basis of these relationships, the coupling was assigned to the proton at C8. With a Q value of −80.0 MHz,[36] McConnell's relation indicates 0.22 π-spin density at C8. Using Bernhard's relation with Q^{π}_{dip}=38.7 MHz, [37] the spin density at C8 is indicated to be 0.24. The close similarity of these two spin density estimates indicates no significant bending of the bonds to the center of spin.

Table 5 lists results from a set of molecular orbital calculations showing the predicted couplings for a variety of base-centered structures related to electron loss. Coupling R2 can fit the primary electron loss product, or either of those from N2 H-abstraction, but none of those from electron gain shown in Table 2. However, the N2 H-abstraction products (from amino deprotonation) can be ruled out because there is no evidence for a second large α-coupling from the remaining amino proton. As well, the total spectral width indicated by the EIE in Figures 2 and 3 is much too small to accommodate that expected when the couplings from nitrogens N2 and N3 are included: the actual width is *ca*. 35 Gauss and the predicted width is 48 Gauss from N2 and N3 alone.[38] Thus, the best match to the experimental values is the set of computational results from the primary electron loss product shown as Structure 3.

The last entry in Table 5 shows couplings calculated for $\cdot G^{+}$, the one-electron oxidation product of guanine. Comparison of these to the couplings computed for R2 shows their similarity and the basis for the expectation that EPR patterns from randomly-oriented distributions of the two structures will be difficult to distinguish. For example, the HC8 couplings of the two are nearly the same and both are predicted to exhibit significant coupling to nitrogen nuclei. In the case of $\cdot G^{+}$, both N2 and N3 are predicted to contribute, while only N3 interacts significantly in the R2 structure; however, the total of N2 and N3 in the $\cdot G^{+}$ structure is virtually the same as that from N3 in R2. In an unresolved pattern from randomly–oriented radicals, the effect of one vs.

two nitrogen couplings will appear in the outer wings and will be difficult to distinguish in DNA from which other, overlapping, spectral components also will be present.

Effective simulation of the EPR from randomly-oriented radicals requires not only the hyperfine tensors but also the g-tensor. Accurate measurement of g tensors is challenging, and it was not possible to do so for R2. Computations of g tensors from the $\cdot G^+$ and R2 structures using G03 (results shown in Table 6) predict virtually identical eigenvectors for both, with g_{min} normal to the purine plane and g_{max} virtually along the C6-O6 bond. The computations also predicted significantly larger g shifts for R2 than for $\cdot G^+$ with respective g_{max} values of 2.0079 and 2.0059. (The difference between the two results evidently reflects the larger spin on O6 in the R2 structure, ρ= 0.20 *vs.* ρ=0.15 for $\cdot G^+$.)

While the accuracy of computed g values is largely untested, the predicted eigenvectors should be reliable inasmuch as they primarily reflect molecular symmetries. Probably the most accurate available g values for guanine oxidation products are those reported by Weiland, et al. from measurements at 245 GHz.[39] Their g_{max} value of 2.00438 from the putative $\cdot G^+$ structure suggests that the computed g shifts ($\delta g = g - g_{electron}$) should be scaled by approximately 22/35 ~ 0.6 for that structure. (We note, however, that it is not absolutely certain their product is actually $\cdot G^+$; it might be the R2 structure.) On the basis of its structural similarities to $\cdot G^+$, it seems reasonable to extend the scaling also to R2. The scaling approach provides the set of proposed g tensors for the R2 and $\cdot G^+$ structures that are listed in the lower part of Table 6.

In summary, the experimental results for radical R2 best fit the computational results for the one-electron oxidized product of the N1-deprotonated guanine parent as shown by Structure 2. The results also demonstrate that the R2 structure, equivalent to the N1-deprotonated product of one-electron oxidized guanine ($\cdot G^+$) exhibits hyperfine couplings similar to those of $\cdot G^+$. On the basis of the consistent correlation between the computed and experimental hyperfine couplings, and by use of computational and experimental results, we have proposed g-tensors for both $\cdot G^+$ and R2 as shown in Table 6.

3.3 Radical R3: HC1′ abstraction

Table 7 lists results from the analysis of ENDOR line 3 (Figure 2) attributed to radical R3. (A complete angular dependence plot is in Supplementary Figure S4.) The large and nearly isotropic character is typical of a hydrogen β-coupling, and the relatively small degree of anisotropy (a_{max} - a_{min} ~ 12 MHz) indicates it to be a CCH_β interaction. The EIE pattern from line 3 (Figure 2) indicates no other couplings contributing to its EPR. (This was confirmed by EIE patterns at other orientations.) Thus, radical R3 exhibits only one hyperfine coupling, and that is from a proton as listed in Table 7.

From inspection of Structure 1, it can be seen that the most likely radicals exhibiting a single hydrogen β-coupling are those centered on the ribose moiety. Only the radical from net hydrogen abstraction at C1′ will have a single β-coupling, from HC2′. However, the wellknown geometry dependence of isotropic β-coupling components[40] makes it necessary to consider two other cases: *i.e.*, abstraction of HC2′, leading to possible couplings with HC1′, HC3′, and HO2′; abstraction from HC3′, leading to possible couplings with HC2′, HC4′, and HO3′. To a rough approximation, the eigenvector associated with the largest principal value ($\widehat{V}_{max}$) of a CCH_β interaction indicates the C…H_β direction. In the undamaged molecule, the direction C1′…HC2′ (Table 6) is 9.8° from the experimental $\widehat{V}_{max}$, and that for C2′···HC1′ is 13.1° from $\widehat{V}_{max}$. These close correspondences favor the identity of R3 as either the HC1′- or HC2′-abstraction structures, but provide no evidence for distinguishing between them.

To help with identifying R3, we performed sets of calculations on the radical structures from HC1′ and HC2′ abstraction (Structures 4 and 5). In either case, the net dehydrogenation is expected to cause some—perhaps significant—reorientation of the bonding geometry to the carbon. As a result, the geometry optimization step can lead to reorientation of the ribose unit extensive enough that the correspondence between computed and experimental geometries will be lost. (We note that Miaskiewicz and Osman previously reported a detailed computational study of deoxyribose radicals,[41] and that Luo, *et al*., reported a correspondingly detailed study of ribose radicals.[42] Both previous studies included discussions of the HC1′ and HC2′ dehydrogenation structures. However, our interest is the description of hyperfine couplings of ribose radicals as they might occur in the NaGR system. To do so, we used the crystal coordinates for the computational input data, the NOSYMM keyword as described above in the Experimental section, and partial optimization procedures intended to mimic the restrictions on reorientation imposed by the surroundings in the crystals as described below.) To provide realistic results while reducing the extent of reorientation during the optimization, the initial structures included the guanine unit, but the optimizations were carried out with all guanine atoms frozen in position. As well, the coordinates of ribose atom C5′ were also frozen. The rationale for these choices was that the molecular packing in the crystal significantly reduces the freedom for the molecule to reorient. Thus, freezing the guanine atoms anchors the C1′ end of the ribose, while freezing the C5′ atom anchors the other end as would be expected in the crystal from the hydrogen bond to HO5′.

Table 8 shows results from the calculations. The first entry is the result of simply using the crystal coordinates with no geometry optimization [B3LYP/6-311G(2df,p)] while the second entry shows the results of optimizing the structure [B3LYP/6-311G(2df,p)//6-31G(d,p)] as described above. For HC1′ abstraction, the isotropic coupling to HC2′ is predicted to be smaller than that observed in both cases. With respective angular deviations of 12.6° and 11.2°, the dipolar vectors of the non-optimized and optimized results agree with experiment equally well. For HC2′ abstraction, the isotropic coupling to HC1′ for the non-optimized structure is predicted to be less than that observed, while the HC1′ coupling for the optimized structure is approximately equal to that observed. The predicted dipolar vectors deviate from that observed by 12.8° and 5.2° for the non-optimized and optimized structures, respectively. In the case of HC2′ abstraction, the computations predict significant couplings to HC3′ and HO2′ is both instances. Since both the HC1′- and HC2′-abstraction structures exhibit only β-couplings, it is possible to manipulate their isotropic values by adjusting the molecular geometries. As an example with HC1′ abstraction, rotation of the HC2′, O2′, and HO2′ atoms by 13° about an axis normal to the HC2′-C2′-O2′ plane changes aiso from 51.0 to 71.3 MHz, a value much closer to that observed. Similarly for the structure from HC2′ abstraction, the positions of HO2′ and HC3′ (along with O3′ and HO3′) can be manipulated to make their computed isotropic couplings nearly vanish. (To make the coupling to HC3′ nearly zero requires rotation of HC3′, O3′, and HO3′ by *ca*. 50°, however.)

In view of these possibilities, we conclude that R3 is the product of HC1′ abstraction. The basis for this conclusion is that EPR from the HC2′ abstraction product should exhibit as many as three significant couplings and the data showed no evidence for more than one. Although the possibility exists that the HC2′ abstraction radical's geometry could be such that couplings to both HC3′ and HO2′ are nearly zero, the probability is low for such a fortuitous condition involving two atoms. Finally, we note that the HC1′ abstraction radical is a wellknown product nucleotides and is usually described as the result of one-electron oxidation of the nucleotide followed by deprotonation at the most labile site. [43]

3.4 Radical R4: H-addition to C8

Upon storing the crystals overnight at room temperature, the EPR was dominated by the characteristic spectrum of the guanine C8 H-adduct (Structure 6) as is shown in Figure 5. Analysis of the ENDOR lines led to the hyperfine couplings listed in Table 7. (Supplementary Figure S5 shows a complete angular dependence plot.) These two large β-couplings are consistent with those observed many times before and are included here for completeness. We note that the computed results for this structure shown in Table 2 predict isotropic components of the large β-couplings significantly less than the observed values. This is a discrepancy noted previously for the purine C8 H-addition structure.[12,44] We should note also that there is no evidence this product is protonated at N7 and that the N7-protonated form of the normal guanine base is well known.[45]

3.5 Mechanisms of Radical Formation

Radical R1, the product of net hydrogenation at N7, was present immediately after the irradiation at 10K. Its formation at this very low temperature indicates that little to no activation energy was required for the reaction. We hypothesize that the hydrogenation actually was the product of two steps: electron capture followed by virtually barrier-free protonation. However, there are at least three sites other than N7 suitable as candidates for protonation following electron capture: N1, N3, and O6. Gas phase energy calculations at B3LYP//6-311G(2df,p)/6-31G(2d,p) of an N1-deprotonated guanine electron adduct indicate N7 to be the best proton acceptor of these (in the order N7>N1>O6>N3). Protonation of the electron adduct at N7 lowers the energy by *ca*. 2.7 kcal/mol more than protonation at N1. Moreover, as is shown by Structure 1, N3 is apparently blocked from external protonation by the intramolecular hydrogen bond to HO5′. As well, O6 is hydrogen bonded to HO3′ of a neighboring molecule and a sodium. The sodium is unlikely to move towards O6 and its presence should be a coulombic deterrent for transfer of HO3′ to O6. N1 is hydrogen-bonded to a hydrogen of water and N7 is hydrogen bonded to HO2′ of a neighboring ribose. Apparently, the deprotonation energy of the ribose at HO2′ is comparable to or less than that of water.

Radical R2 is the primary one-electron oxidation product, while R3 is usually regarded as the product of one-electron oxidation followed by deprotonation. Their coexistence as products in the NaGR system indicates a barrier between the two higher than that accessible by thermal energy alone at 10K. Thus, in some cases (*ca*. 1/3; see below), the event of oxidative ionization apparently leaves excitation energy in the system sufficient for it to access the deprotonated state. It is interesting that the deprotonation occurs at C1′ rather than at the amino. However, this is supported by gas phase energy calculations at B3LYP//6-311G(2df,p)/6-31G(2d,p) which predict the energy of the full structure (N1-deprotonated guanine plus ribose) to be lower for deprotonation at C1′ than at C2′ or the amino by *ca*. 5.5 kcal/mol.

Radical R4 was not detectible in the low temperature spectra. Its presence after warming the crystals to room temperature indicates it to be a secondary product of the low-temperature precursors. We note that computations predict the C8 H-addition product to be the most stable of all those listed in Table 2: its energy is approximately 15 kcal/mol lower than that of the N7 addition product.

Use of the WINSIM-based spectrum-fitting procedure for nine distinct crystal orientations indicated the initial radical concentrations after irradiation at 10K to be 60% R1, 27% R2 and 13% R3, with *ca*. 10% uncertainty. Thus, within this range of uncertainty, the radical balance is approximately equal between oxidation and reduction products. A more complete description of reaction mechanisms in the NaGR system will appear elsewhere.

4. Summary and Conclusions

In summary, therefore, x-irradiation of sodium guanosine dihydrate crystals at 10 K led to the detection of three radical products. R1, the product of net hydrogenation at N7 of the N1-deprotonated guanine parent evidently formed via electron addition followed by proton transfer from a neighboring molecule. HO2′ of a neighboring ribose unit is 1.98 Å from N7 and most likely is the source of the proton. The magnetic parameters of R1 indicate extreme bending of the bonds to N7 and C8. In this highly unusual geometry, the bending at C8 is sufficiently extreme to make the isotropic component of the α-coupling to HC8 take on a positive sign and magnitude greater than the usual planar case. The net result is that all components of the HC8 α-coupling are positive, a characteristic in sharp contrast to the usual case in which all are negative.

Both R2 and R3 evidently are the products of one-electron oxidation and are present in the approximate 2:1 ratio. R2 is the primary oxidation product in NaGR and is equivalent to the N1-deprotonated product of the primary guanine cation. R3, the product of net hydrogen abstraction from C1′ of the ribose, most likely is the result of one-electron oxidation followed by deprotonation. The presence of both the primary oxidation product and its deprotonated successor demonstrates that both are stably trapped in the NaGR host system, and indicates that there is an energy barrier to the deprotonation process. A postulate based on this observation is that the event of electron loss leaves sufficient molecular energy available to produce deprotonation in some cases and not in others.

Radical R4, the product of net hydrogen addition to C8 was detected only after warming the crystals to room temperature overnight. Evidently it is a secondary product of a low-temperature precursor.

Supplementary Material

Refer to Web version on PubMed Central for supplementary material.

Acknowledgements

This work was supported in part by NIH grant CA36810, and by the Research Program Enhancement fund of Georgia State University.

References

1. Pullman B, Pullman A. Proc. Natl. Acad. Sci. U. S. A 1958;44:1197. [PubMed: 16590332]
2. Gräslund A, Ehrenberg A, Rüpprecht A, Ström G. Biochim. Biophys. Acta 1971;254:172. [PubMed: 4332768]
3. Close DM, Sagstuen E, Nelson WH. J. Chem. Phys 1985;82:4386.
4. Rakvin B, Herak JN, Voit K, Hüttermann J. Radiat. Env. Biophys 1987;26:1. [PubMed: 3035602]
5. Hole EO, Nelson WH, Close DM, Sagstuen E. J. Chem. Phys 1987;86:5218.
6. Candeias LP, Steenken S. J. Am. Chem. Soc 1989;111:1094.
7. Colson AO, Besler B, Close DM, Sevilla MD. J. Phys. Chem 1992;96:661.
8. Luo Q, Li QS, Xie Y, Schaefer HF. Collect. Czech. Chem. Commun 2005;70:826.Mundy CJ, Colvin ME, Quong AA. J. Phys. Chem. A 2002;106:10063.
9. Hutter M, Clark T. J. Am. Chem. Soc 1996;118:7574.
10. Li X, Cai Z, Sevilla MD. J. Phys. Chem. B 2001;105:10115.
11. Hole EO, Sagstuen E, Nelson WH, Close DM. Radiat. Res 1992;129:1. [PubMed: 1309400]
12. Tokdemir S, Nelson WH. J. Phys. Chem. A 2006;110:6552. [PubMed: 16706414]
13. Deuterated crystals were prepared in a similar manner using D_20 and NaOD. However, NMR analysis of these indicated virtually full exchange of the guanine amino protons and >60% exchange of HC8.

It was not possible to verify the degree to which the ribose OH protons were exchanged. Although spectra from the deuterated and normal crystals were different, the mixed and uncertain degree of exchange made them useful only for concluding that none of the ENDOR lines detected were from the amino protons.

14. Nagashima N, Tsujita H, Iitaka Y. Anal. Sci 1992;8:581.
15. Nelson WH. J. Magn. Reson 1980;38:71.
16. Schonland DS. Proc. Phys. Soc 1959;73:788.
17. Busing, WR.; Martin, KO.; Levy, HA. Oak Ridge Natl. Lab.; Oak Ridge,TN: 1964. “ORFFE--a Fortran crystallographic function and error program”.
18. Frisch, MJ.; Trucks, GW.; Schlegel, HB.; Scuseria, GE.; Robb, MA.; Cheeseman, JR.; Montgomery, JA., Jr.; Vreven, T.; Kudin, KN.; Burant, JC.; Millam, JM.; Iyengar, SS.; Tomasi, J.; Barone, V.; Mennucci, B.; Cossi, M.; Scalmani, G.; Rega, N.; Petersson, GA.; Nakatsuji, H.; Hada, M.; Ehara, M.; Toyota, K.; Fukuda, R.; Hasegawa, J.; Ishida, M.; Nakajima, T.; Honda, Y.; Kitao, O.; Nakai, H.; Klene, M.; Li, X.; Knox, JE.; Hratchian, HP.; Cross, JB.; Adamo, C.; Jaramillo, J.; Gomperts, R.; Stratmann, RE.; Yazyev, O.; Austin, AJ.; Cammi, R.; Pomelli, C.; Ochterski, JW.; Ayala, PY.; Morokuma, K.; Voth, GA.; Salvador, P.; Dannenberg, JJ.; Zakrzewski, VG.; Dapprich, S.; Daniels, AD.; Strain, MC.; Farkas, O.; Malick, DK.; Rabuck, AD.; Raghavachari, K.; Foresman, JB.; Ortiz, JV.; Cui, Q.; Baboul, AG.; Clifford, S.; Cioslowski, J.; Stefanov, BB.; Liu, G.; Liashenko, A.; Piskorz, P.; Komaromi, I.; Martin, RL.; Fox, DJ.; Keith, T.; Al-Laham, MA.; Peng, CY.; Nanayakkara, A.; Challacombe, M.; Gill, PMW.; Johnson, B.; Chen, W.; Wong, MW.; Gonzalez, C.; Pople, JA. Gaussian 03. Gaussian Inc.; Pittsburgh PA: 2003. Rev. B.04 ed.
19. Pauwels E, Van Speybroeck V, Vanhaelewyn G, Callens F, Waroquier M. Int. J. Quantum Chem 2004;99:102.
20. Rienstra-Kiracofe JC, Tschumper GS, Schaefer HF, Nandi S, Ellison GB. Chem. Rev 2002;102:231. [PubMed: 11782134]
21. Li X, Cai Z, Sevilla MD. J. Phys. Chem. A 2002;106:1596.
22. Roehrig GH, Oyler NA, Adamowicz L. Chem. Phys. Lett 1994;225:265.Haranczyk M, Gutowski M. J. Am. Chem. Soc 2005;127:699. [PubMed: 15643895]
23. Hendricks JH, Lyapustina SA, de Clercq HL, Bowen KH. J. Chem. Phys 1998;108:8.
24. Törring JT, Un S, Knupling M, Plato M, Möbius K. J. Chem. Phys 1997;107:3905.Jayatilaka D. J. Chem. Phys 1998;108:7587.
25. Duling DR, Motten AG, Mason RP. J. Magn. Reson 1988;77:504.Duling DR. J. Magn. Reson 1994;B104:105.
26. The off-axis positions give data from two magnetic sites and therefore provide data for two distinct positions.
27. Tokdemir S, Nelson WH. J. Phys. Chem. A 2005;109:8732. [PubMed: 16834275]
28. Typical α-couplings have two dipolar components of roughly equal magnitude but opposite sign and a third component near zero. The “dipolar” value can be indicated by the average of the magnitudes of the two large values.
29. McConnell HM, Strathdee J. Mol. Phys 1959;2:129.
30. Erling PA, Nelson WH. J. Phys. Chem. A 2004;108:7591.
31. We note that optimization of the N7-hydrogenation structure using 6-31+G(d,p) or 6-31++G(d,p) basis sets led to a geometry with the N7 hydrogen bent to the side of the molecular plane opposite to that shown in Figure 3. That is, HN7 and HN9 were bent to one side of the plane and HC8 to the other. However, optimization with diffuse functions within a dielectric field using the PCM method led to a structure like that in Figure 3. For this and other reasons described in the Experimental section, we conclude that computations without diffuse functions reliably describe optimized structures within the NaGR system.
32. McConnell HM, Chesnut DB. J. Chem. Phys 1958;28:107.
33. The normal experimental procedure cannot establish the absolute sign of the coupling components. However, the results correctly provide their relative signs.
34. This result requires rearrangement of the eigenvector signs by multiplying the x components by -1. This transformation is consistent with the magnetic site symmetry of the orthorhombic system.

35. Dobbs, AJ.; Gilbert, BC.; Norman, ROC. J. Chem. Soc. D. 1969. p. 1353Fessenden, RW.; Schuler, RH. J. Chem. Phys. 1965. p. 2704

36. Ngo Q, Budzinski EE, Box HC. J. Chem. Phys 1974;60:3373.Nelson, WH.; Gill, CD. Mol. Phys. 1978. p. 1779

37. Bernhard WA. J. Chem. Phys 1984;81:5928.Gordy, W. Theory and Applications of Electron Spin Resonance. Wiley; New York: 1980.

38. The predicted width was estimated from the maximum value of the computed couplings (*ca*. 20 Gauss for N2 plus 10 Gauss for N3) times the cosine of the angle between <b> and the normal to the ring, *ca*. 0.8.

39. Weiland B, Hüttermann J, Van Tol J. Acta Chem. Scand 1997;51:585.

40. Derbyshire W. Mol. Phys 1962;5:225.

41. Miaskiewicz K, Osman R. J. Am. Chem. Soc 1994;116:232.

42. Luo N, Litvin A, Osman R. J. Phys. Chem. A 1999;103:592.

43. Hole EO, Nelson WH, Sagstuen E, Close DM. Radiat. Res 1992;129:119. [PubMed: 1310357]Close DM, Nelson WH, Sagstuen E, Hole EO. Radiat. Res 1994;137:300. [PubMed: 8146272]Weiland B, Hüttermann J, Malone ME, Cullis PM. Int. J. Radiat. Biol 1996;70:327. [PubMed: 8800204]

44. Wetmore SD, Boyd RJ, Eriksson LA. J. Phys. Chem. B 1998;102:9332.

45. Alexander C Jr. Gordy W. Proc. Natl. Acad. Sci. U. S. A 1967;58:1279. [PubMed: 16591568]Nelson WH, Hole EO, Sagstuen E, Close DM. Int. J. Radiat. Biol 1988;54:963. [PubMed: 2903893]Close DM, Sagstuen E, Nelson WH. Radiat. Res 1988;116:379. [PubMed: 2849779]

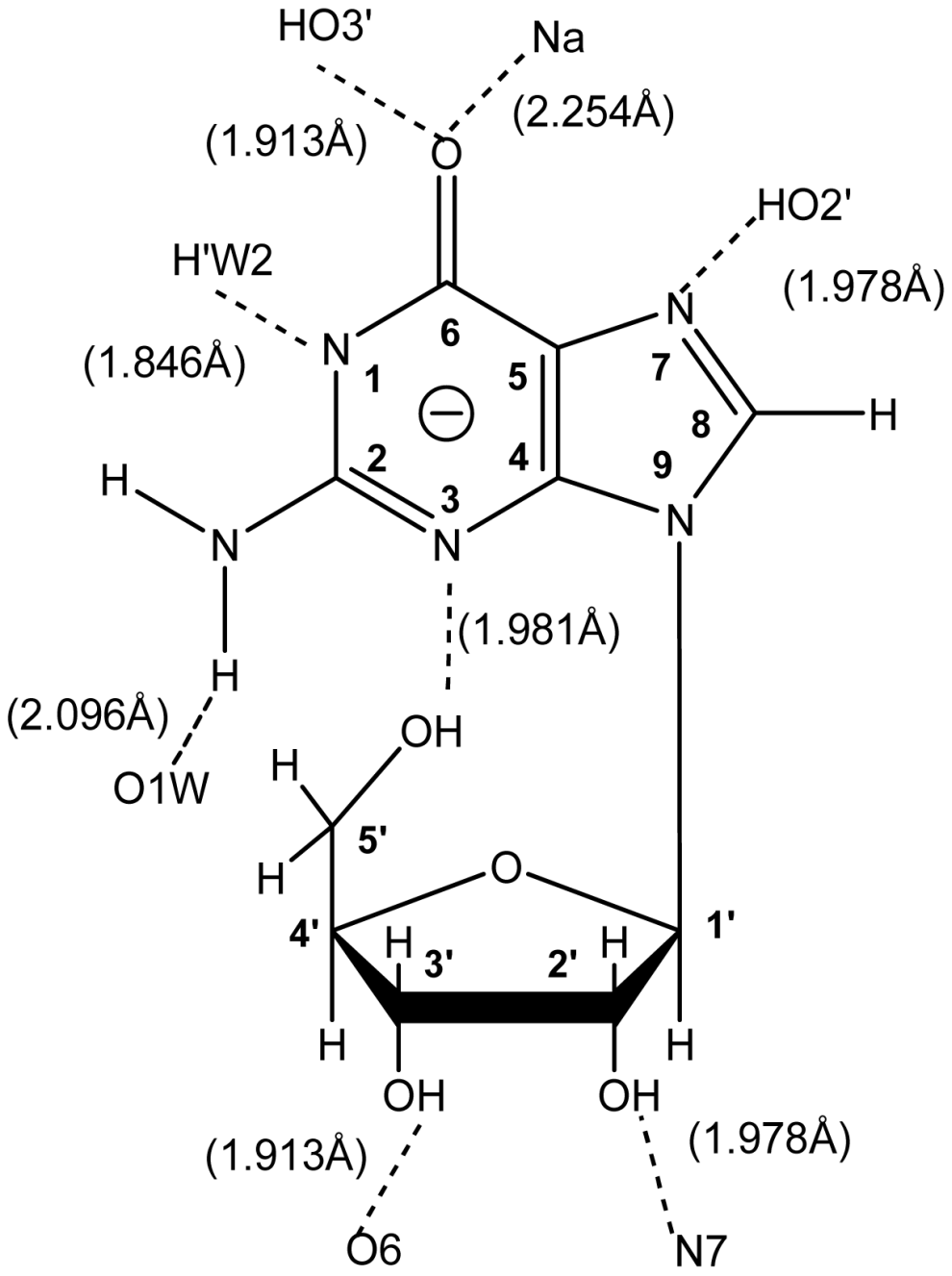

Structure 1.
N1-deprotonated guanosine as present in NaGR crystals. The dotted lines indicate the system of hydrogen bonds and close contacts in the crystals.

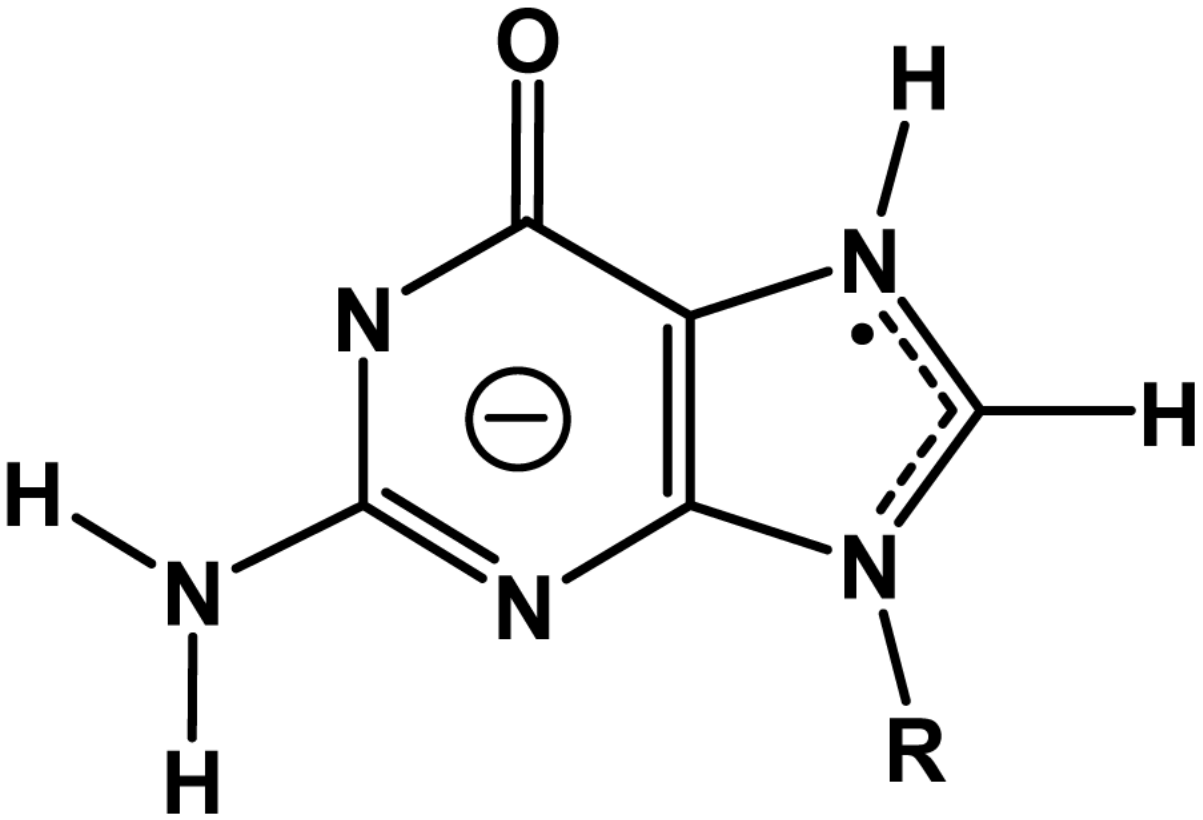

Structure 2.
Radical R1, the N7-protonated electron gain product of NaGR.

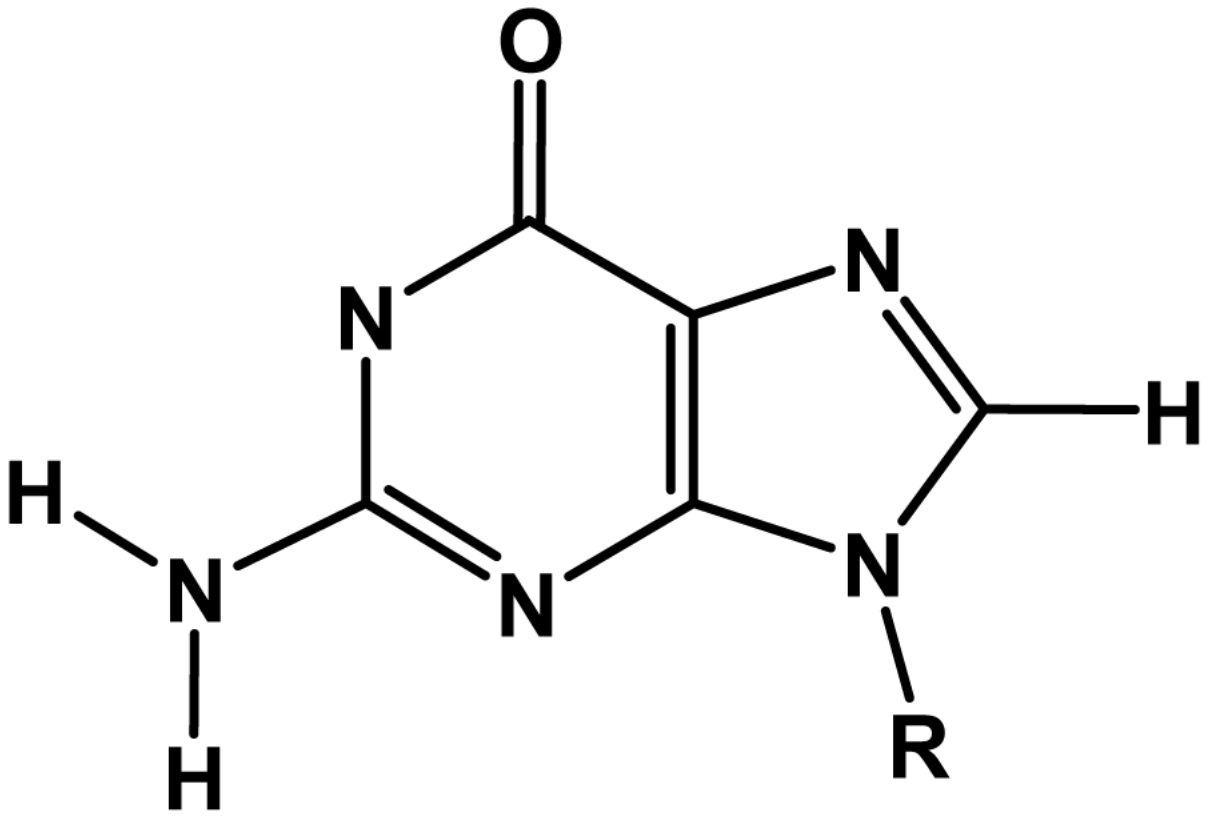

Structure 3.
Radical R2, the electron-loss product in NaGR.

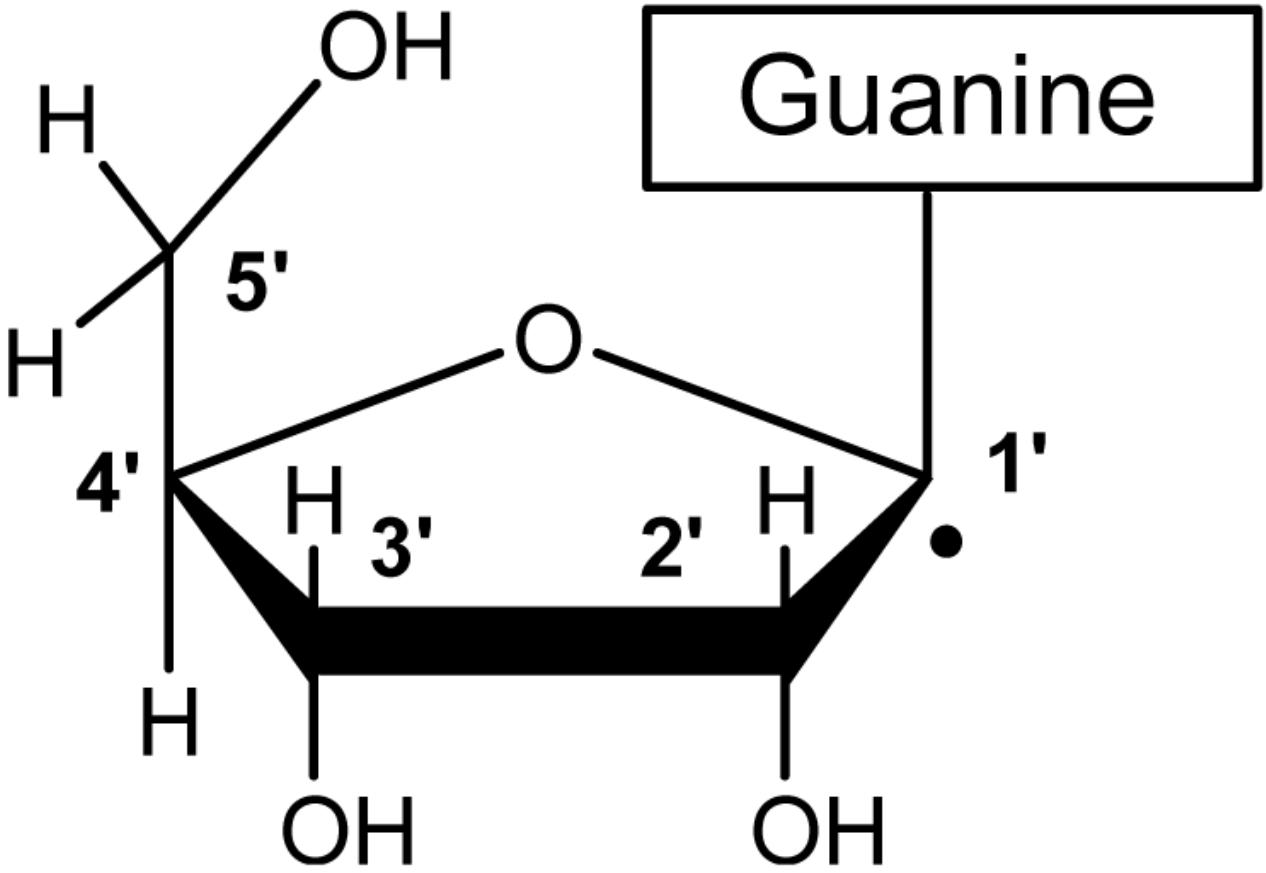

Structure 4.
(left), the product of HC1′ abstraction.

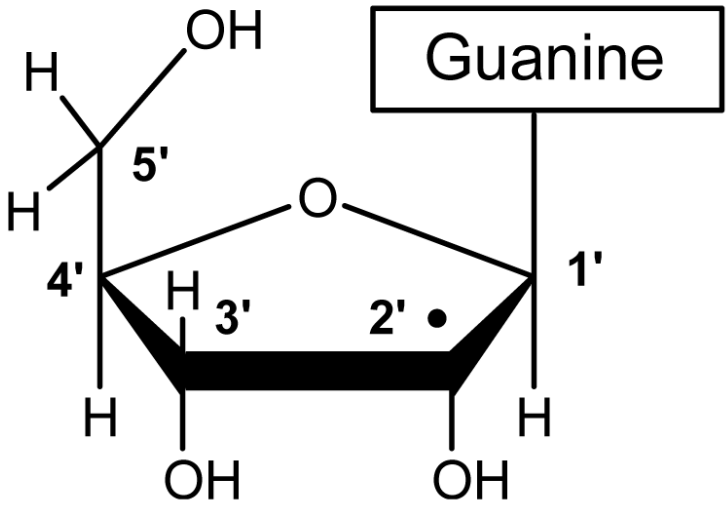

Structure 5.
(right), the product of HC2′ abstraction

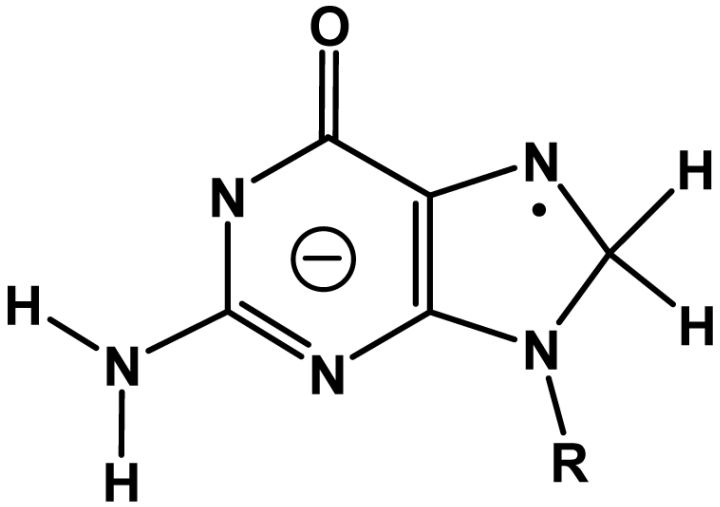

Structure 6.
Guanine C8 H-adduct.

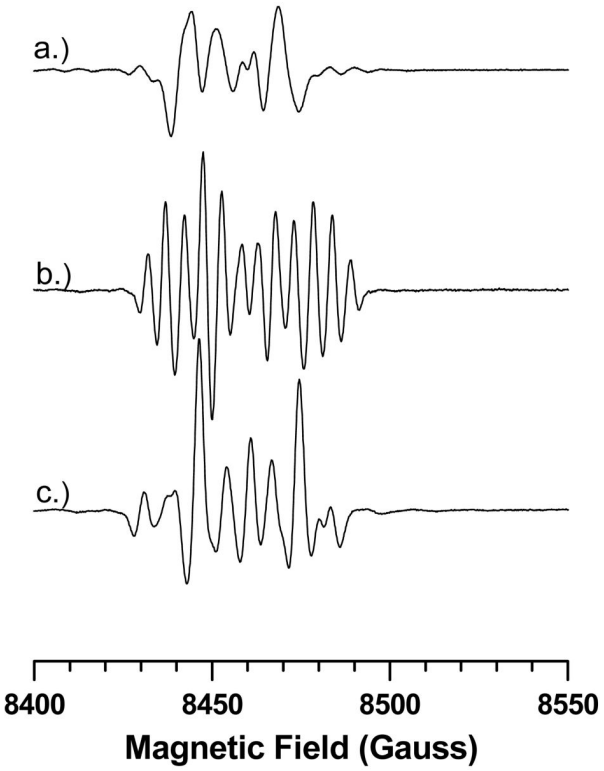

Figure 1.
EPR spectra (second derivative) with the magnetic field along the (a) <a>, (b) <b> and (c) <c> crystallographic axes for the Na^{+}·guanosine^{-}·$2H_2O$ (NaGR) single crystals x- irradiated and recorded at 10K.

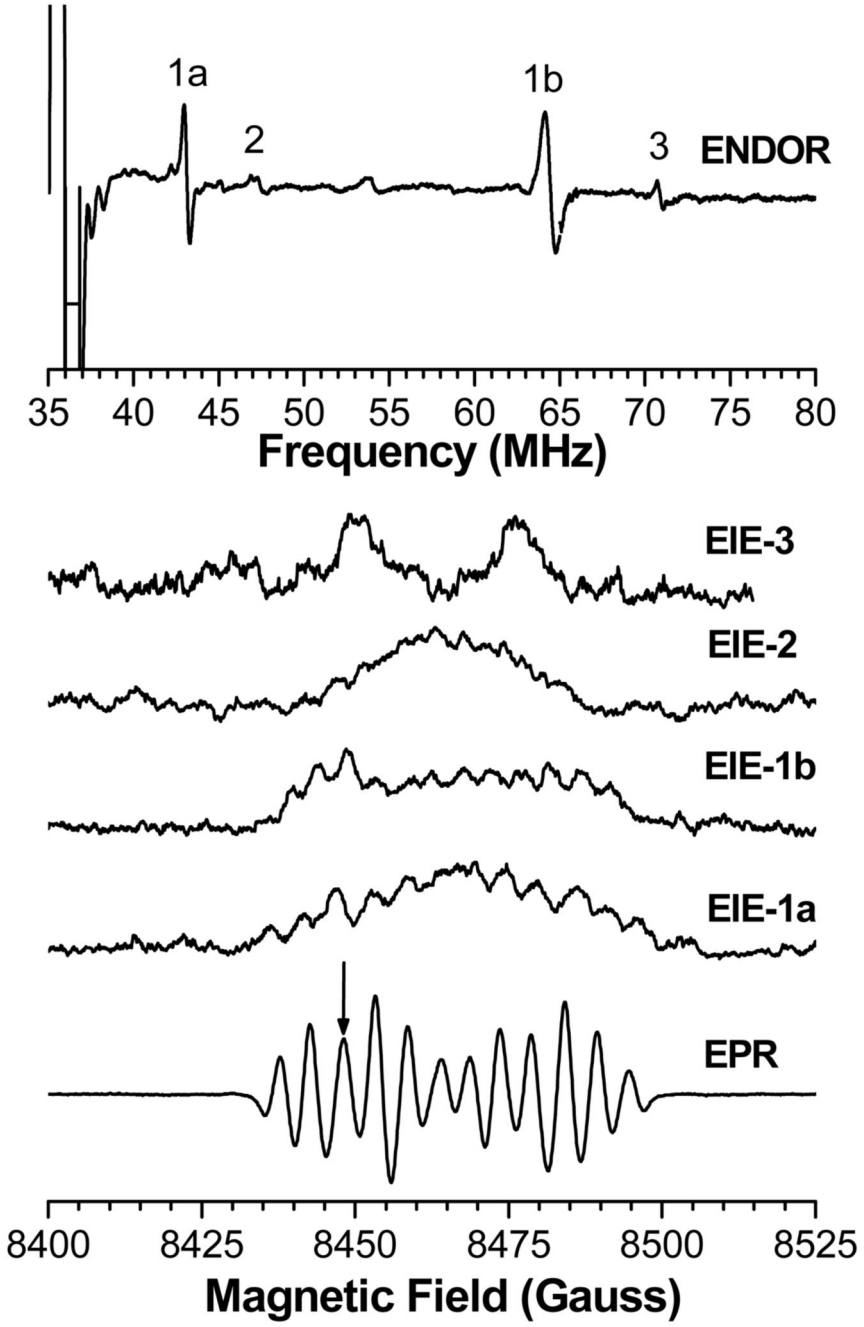

Figure 2.
ENDOR, EIE and EPR spectra (second derivative) from NaGR with the magnetic field along the crystallographic <b> axis following x-irradiation and observation at 10 K. The arrow on the EPR pattern indicates the field setting for the ENDOR pattern shown.

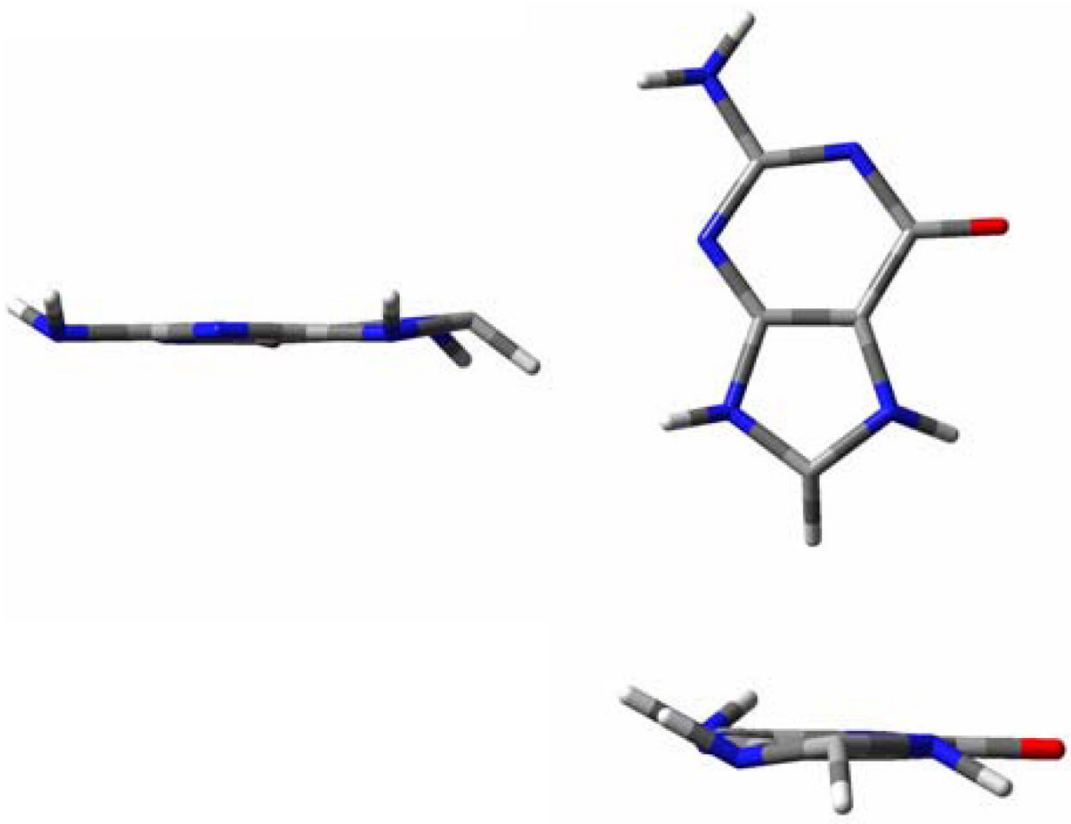

Figure 3.
Illustrations of the as-optimized structure for R1: upper left, view approximately along N9-HN9; upper right, facial view; lower right, view approximately along C8-HC8.

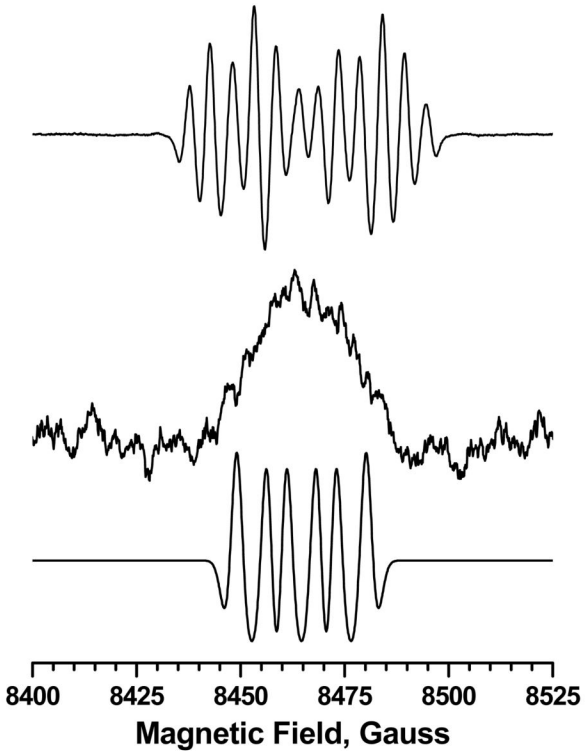

Figure 4.
EIE from R2 (center) with the magnetic field along <b> compared with the simulated second-derivative EPR (bottom) for that radical alone and the experimental spectrum (top).

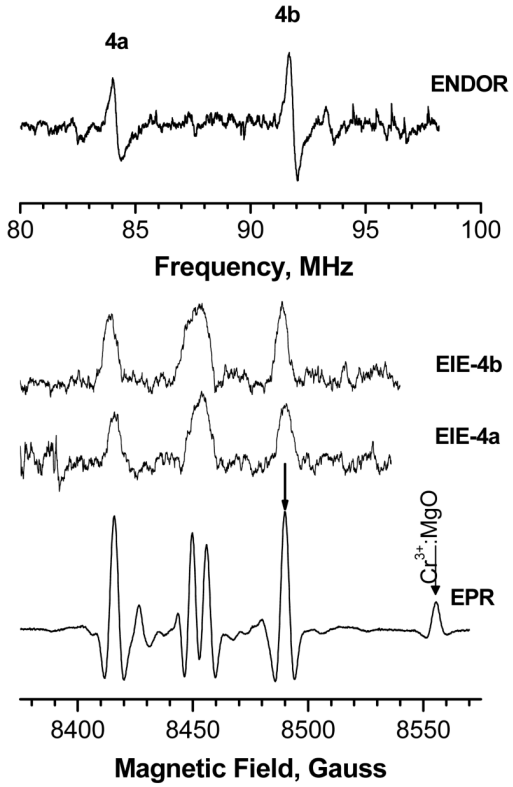

Figure 5.
ENDOR, EIE and EPR (second derivative) spectra from NaGR single crystals irradiated at 10 K and recorded at 298 K after over storage at room temperature. The magnetic field is 30° from the crystallographic <c> axis in the <bc> plane. This orientation is 3° from the guanine ring plane for one of the sites.

Table 1

Experimental hyperfine couplings[a] for radical R1 in crystals of Na^+·guanosine$^-$·$2H_2O$ X-irradiated at 10K. All coupling values are in MHz

Coupling	Isotropic value	Principal values	Eigenvectors		
			x	*y*	*z*
$R1_a$	62.2(2)	84.8(2)	−0.290(6)	−0.111(5)	0.951(3)
		60.8(5)	−0.489(8)	0.871(3)	−0.048(4)
		41.0(5)	0.823(1)	0.479(8)	0.307(4)
$R1_b$	12.9(3)	23.7(3)	0.637(8)	0.153(16)	0.756(5)
		16.5(2)	0.205(23)	0.911(6)	−0.357(9)
		−1.5(3)	0.743(10)	−0.382(21)	−0.549(7)
N7[b]	29.5	48.0		normal to the molecular plane	
		20.3		parallel to the molecular plane	
		20.3		parallel to the molecular plane	
N9[b]	8.8	23.3		normal to the molecular plane	
		1.5		parallel to the molecular plane	
		1.5		parallel to the molecular plane	
Crystallographic directions:					
Normal to the purine plane[c]			0.3217	−0.7957	0.5132
Bisector to C5-N7-C8			0.6132	0.5839	0.5320
C8-H bond direction			0.4910	−0.3222	−0.8094
N7 to neighboring HO2			0.6970	0.4799	0.5328

[a] Numbers in parentheses are the standard deviations of the last quoted digit(s).

[b] Nitrogen couplings were estimated by EPR spectrum simulations; see the text for details.

[c] Normal to the least-squares plane through all ring atoms (N1, C2,…,C8, N9).

b_0	b_+	Radical	Atom	a_{iso}	b_-	b_0	b_+
−0.4	1.4	O6H-addition (a) 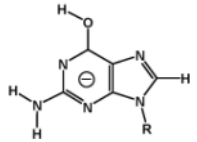	N2-H	5.6	−1.1	−0.7	−1.8
−0.5	1.5		N2-H'	2.4	−1.5	−0.8	2.3
−2.6	15.9		C8-H	31.4	−15.8	−0.3	16.1
−0.5	1.1		O6-H	−2.5	−4.2	−3.8	7.9
−15.4	31.4		N7	7.9	−7.8	−7.2	15.0
			N3	3.6	−4.0	−3.8	7.8

J Phys Chem B. Author manuscript; available in PMC 2009 July 28.

b_0	b_+	Radical	Atom	a_{iso}	b_-	b_0	b_+
−4.6	12.2	O6H-addition (b)	N2-H	5.7	−1.1	−0.7	−1.8
−4.4	10.2		N2-H'	2.7	−1.4	−0.7	2.1
−2.4	7.8		C8-H	50.0	−16.7	−1.0	17.7
−0.1	4.0		O6-H	−2.5	−3.9	−1.1	5.0
0.1	1.3		N7	9.3	−9.5	−9.0	18.5
−4.9	10.4		N3	3.8	−0.8	−0.7	1.5

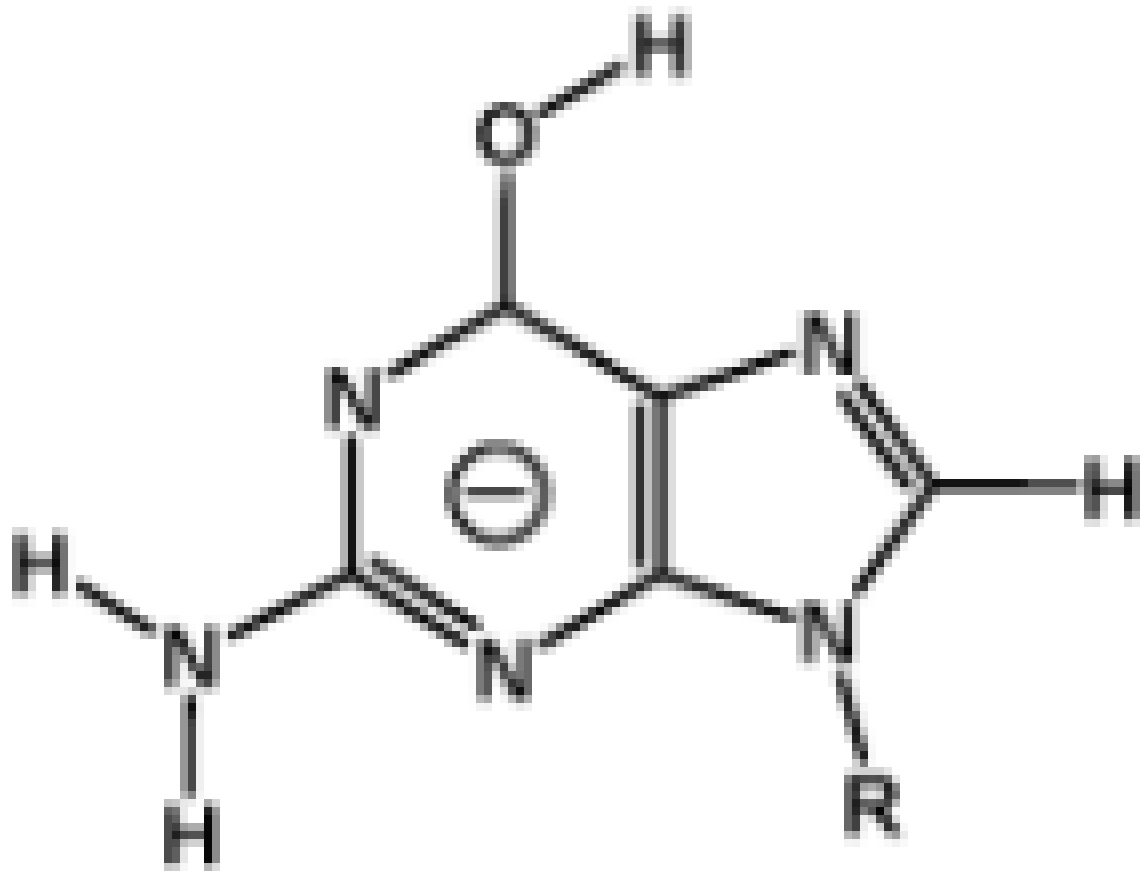

b_0	b_+	Radical	Atom	a_{iso}	b_-	b_0	b_+
−2.1	7.2	N7H-addition	N2-H	0.5	−0.4	−0.2	0.6
−4.1	9.2		N2-H'	0.7	−0.5	−0.3	0.8
−5.0	12.1		C8-H	83.5	−20.3	−3.5	23.7
0.0	2.7		N7-H	14.1	−14.1	−5.5	19.6
−4.7	10.1		N7	35.0	−12.5	−11.8	24.3
0.1	1.2		N9	1.2	−8.5	−8.4	16.9

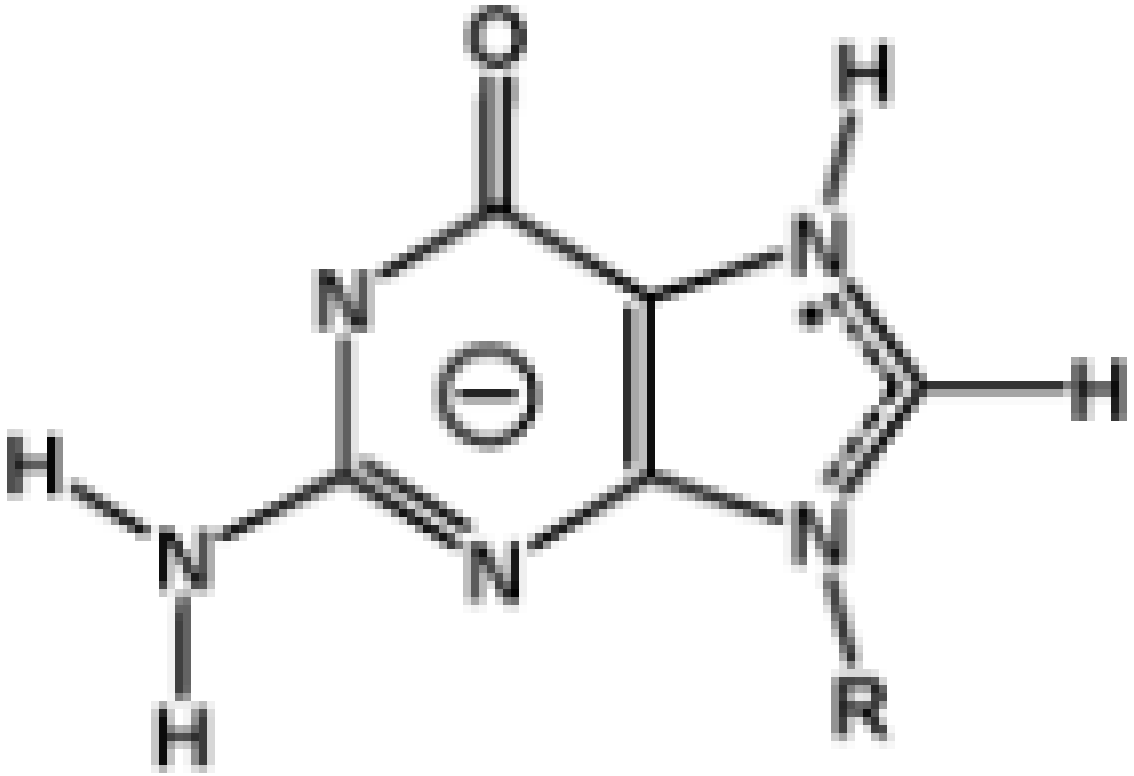

J Phys Chem B. Author manuscript; available in PMC 2009 July 28.

b_0	b_+	Radical	Atom	a_{iso}	b_-	b_0	b_+
−0.5	1.5	C8H-addition 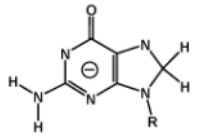	N2-H	3.6	−1.6	−1.0	2.6
−0.6	1.4		N2-H'	3.0	−1.8	−1.1	2.9
−1.6	5.6		C8-H	66.0	−3.5	−2.4	5.9
0.1	17.9		C8-H'	90.7	−3.5	−2.3	5.8
5.0	5.3		N7	17.8	−24.2	−23.5	47.6
−4.8	10.1		N9	4.5	−3.5	−3.1	6.6

J Phys Chem B. Author manuscript; available in PMC 2009 July 28.

Radical	b_0	b_+	Atom	a_{iso}	b_-	b_0	b_+
	−1.5	4.3					
	−2.0	5.0					
	−1.7	4.9					
	−1.2	3.7					
	−2.7	5.9					
						2.9	

Table 3

Comparison of experimental and computed couplings for R1.[a]

Atom	Coupling Values	a_{iso}	b_{dip}	Eigenvectors *x*	*y*	*z*	$\Delta\varphi$[b]
Experiment							
	84.80		22.60	−0.2900	−0.1110	0.9510	
$R1_a$	60.80	62.20	−1.40	−0.4890	0.8710	−0.0480	
HC8	41.00		−21.20	0.8230	0.4790	0.3070	
	23.70		10.80	0.6370	0.1530	0.7560	
$R1_b$	16.50	12.90	3.60	0.2050	0.9110	−0.3570	
HN7	−1.50		−14.40	0.7430	−0.3820	−0.5490	
As-optimized: HC8 @ 45.05°, HN7 @ 31.47°							
	107.20		23.74	−0.1649	−0.1201	0.9790	*7.2*
HC8	79.97	83.45	−3.49	−0.6038	−0.0039	0.9790	*8.2*
	63.20		−20.25	0.7799	0.5917	0.2039	*8.9*
	33.73		19.63	0.7404	0.2270	0.6327	*10.4*
HN7	8.62	14.10	−5.48	−0.0862	0.9655	−0.2456	*18.3*
	−0.05		−14.15	−0.6666	0.1273	0.7344	*18.7*
Adjusted: HC8 @ 40°, HN7 @ 31.47°							
	88.50		24.19	−0.1987	−0.0799	0.9768	*5.5*
HC8	61.82	64.30	−2.49	−0.5997	0.7982	−0.0567	*7.6*
	42.60		−21.71	0.7752	0.5970	0.2065	*9.1*
	32.57		19.49	0.7421	0.2472	0.6230	*11.0*
HN7	7.81	13.08	−5.28	−0.1017	0.9603	−0.2599	*18.8*
	−1.14		−14.22	−0.6625	0.1295	0.7378	*18.8*

[a] Coupling values in MHz.

[b] Angular difference with experimental vectors (degrees).

Table 4

Hyperfine couplings[a] for radical R2 in crystals of Na^+ guanosine$^-$ $2H_2O$ (NaGR) x-irradiated at 10 K. All coupling values are in MHz.

Coupling	Isotropic value	Principal values	Eigenvectors		
			x	*y*	*z*
R2 (HC8)	−17.5(3)	−26.7(8)	0.780(1)	0.505(2)	0.369(1)
		−18.3(1)	−0.363(2)	0.847(1)	−0.389(2)
		−7.4(0)	0.509(1)	−0.170(2)	−0.844(1)
N3[b]	14.7	42.0	normal to the molecular plane		
		1.1	parallel to the molecular plane		
		1.1	parallel to the molecular plane		
Crystallographic directions:					
Normal to the molecular plane[c]			0.3217	−0.7957	0.5132
C8-H bond direction			0.4910	−0.3222	−0.8094

[a] The numbers in parentheses are the standard deviations of the last quoted digit(s)

[b] Nitrogen couplings were estimated by EPR spectrum simulations; see the text for details

[c] Normal to the least-squares plane through all ring atoms (N1, C2,…,C8, N9).

Table 5

Computed hyperfine couplings for guanine-centered radical structures in NaGR related to electron loss. All coupling values are in MHz. (For all computations in this table, R was a hydrogen.)

Radical	Atom	a_{iso}	b_{-}	b_{0}	b_{+}
Electron loss 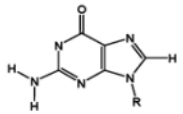	N2-H	−3.62	−2.42	−1.01	3.43
	N2-H'	−4.90	−3.65	−1.39	5.04
	C8-H	−20.68	−12.07	−0.71	12.78
	N1	−0.57	−0.12	−0.03	0.15
	N2	1.49	−2.82	−2.45	5.27
	N3	10.51	−15.01	−14.77	29.78
N2H-abstraction 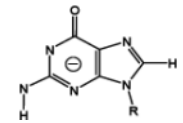	N2-H'	−34.83	−31.67	−5.24	36.91
	C8-H	−12.44	−7.50	0.02	7.48
	N1	2.79	−4.90	−4.49	9.39
	N2	14.61	−26.73	−25.75	52.48
	N3	7.63	−11.86	−11.24	21.1
N2H'-abstraction 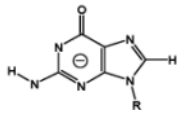	N2-H	−35.42	−31.31	−6.02	37.33
	C8-H	−11.86	−7.17	0.03	7.14
	N1	3.09	−5.71	−5.28	10.99
	N2	15.42	−27.67	−26.76	54.43
	N3	7.22	−10.86	−10.22	21.08
$•G^{+}$ 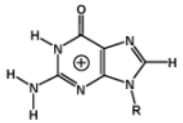	N2-H	−7.18	−3.92	−2.68	6.60
	N2-H'	−8.22	−6.55	−1.72	8.27
	C8-H	−22.76	−12.91	−1.42	14.33
	N1	−2.24	−1.70	0.72	0.98
	N2	3.38	−5.19	−4.89	10.08
	N3	6.84	−10.45	−10.18	20.63

Table 6

Calculated g-tensors using G03 with •G^+ and R2 structures optimized from initial crystallographic coordinates of NaGR.

Radical	Isotropic value	Principal value	Eigenvectors		
			x	*y*	*z*
Computed g values					
		2.0059	0.9124	0.3526	0.2076
•G^+	2.0038	2.0033	0.3310	−0.3378	−0.8811
		2.0024	0.2406	−0.8726	0.4250
		2.0079	0.8884	0.4380	0.1372
R2	2.0048	2.0045	0.3357	−0.4163	−0.8450
		2.0022	0.3129	−0.7968	0.5169
Crystallographic ring normal			0.3212	−0.7961	0.5130
C6-O6 direction			0.8679	0.4630	0.1802
Proposed g values					
		2.0044	*Parallel to C6-O6*		
•G^+	2.0032	2.0029	*Normal to the other directions*		
		2.0024	*Normal to the ring*		
		2.0055	*Parallel to C6-O6*		
R2	2.0038	2.0036	*Normal to the other directions*		
		2.0022	*Normal to the ring*		

Table 7

Experimental hyperfine parameters[a] for radicals R3 and R4 in crystals of NaGR x-irradiated at 10 K. All coupling values are in MHz.

Tensor	Isotropic value	Principal value	Eigenvectors		
			x	*y*	*z*
R3	74.2(2)	81.3(2)	0.270(24)	−0.206(14)	0.941(16)
		72.6(1)	0.864(19)	−0.381(18)	−0.331(9)
		68.7(5)	0.426(3)	0.902(26)	0.075(9)
Crystallographic directions:					
C1'…HC2' direction			−0.1168	0.1427	−0.9829
C2'…HC1' direction			0.1667	0.0071	0.9860
$R4_a$	96.0(2)	102.0(2)	0.796(12)	−0.507(23)	−0.331(54)
		93.7(2)	0.583(14)	0.789(35)	0.194(76)
		92.3(2)	0.163(13)	−0.347(86)	0.924(19)
$R4_b$	112.1(2)	117.7(2)	0.592(10)	−0.262(31)	−0.762(61)
		109.9(2)	0.744(20)	−0.185(81)	0.642(15)
		108.6(2)	0.309(8)	0.947(14)	−0.085(64)

[a] The numbers in parentheses are the standard deviations of the last quoted digit(s)

Table 8

Experimental and computed hyperfine couplings for R3. All coupling values are in MHz.

Atom	Principal Values	a_{iso}	a_{dip}	Eigenvectors			$\Delta\phi^a$
				x	*y*	*z*	
Experimental, R3							
	81.29		7.08	0.2696	−0.2055	0.9408	
	72.63	74.21	−1.59	0.8635	−0.3809	−0.3307	
	68.72		−5.49	0.4263	0.9015	0.0748	
Computed using crystal coordinates without optimization:							
HC1' abstraction							
	54.59		7.54	0.0631	−0.1496	0.9867	*12.6*
HC2'	46.15	47.05	−0.91	0.9379	−0.3290	−0.1099	*13.7*
	40.42		−6.63	0.3411	0.9324	0.1196	*5.8*
HC2' abstraction							
	67.53		7.51	0.1832	−0.0049	0.9831	*12.8*
HC1'	57.78	60.02	−2.24	0.7382	−0.6597	−0.1409	*20.7*
	54.74		−5.28	0.6493	0.7515	−0.1172	*19.0*
	57.53		24.27	0.3346	−0.0514	0.9410	
HO2'	24.10	33.26	−9.16	0.8856	−0.3243	−0.3326	
	18.15		15.11	0.3346	−0.0514	0.9410	
	33.18		11.50	−0.3201	0.7727	−0.5481	
HC3'	17.27	21.68	−4.41	−0.6270	0.2609	0.7340	
	14.59		−7.09	0.7102	0.5786	0.4010	
Optimized with purine and C5' frozen:							
HC1' abstraction							
	58.09		7.11	0.3738	−0.3499	0.8590	*11.2*
HC2'	49.37	50.98	−1.61	0.8564	−0.2254	−0.4645	*11.8*
	45.48		−5.51	0.3561	0.9093	0.2154	*9.0*
HC1' abstraction: HC2', O2', and HO2' rotated by -13°							
	79.07		7.82	0.3947	−0.2836	0.8739	*9.3*
HC2'	70.06	71.25	−1.19	0.8280	−0.3025	−0.4721	*9.5*
	64.63		−6.63	0.3983	0.9100	0.1155	*2.8*

Atom	Principal Values	a_{iso}	a_{dip}	Eigenvectors			$\Delta\phi^a$
				x	*y*	*z*	
HC2' abstraction							
	85.61		8.91	0.3058	−0.1236	0.9440	*5.2*
HC1'	72.75	76.70	−3.95	−0.5325	0.7997	0.2772	*31.1*
	71.73		−4.97	0.7892	0.5875	−0.1788	*31.5*
	41.60		8.94	0.3999	0.5890	0.7023	
HC3'	29.01	32.66	−3.64	0.8933	−0.0790	−0.4425	
	27.36		−5.30	−0.2051	0.8043	−0.5577	
	36.05		19.96	0.8491	0.4908	0.1952	
HO2'	7.84	16.09	−8.25	−0.3798	0.3106	0.8713	
	4.38		−11.71	−0.3670	0.8140	−0.4502	

[a] Angular difference (degrees) from experimental values.